ACS APPLIED MATERIALS & INTERFACES

Research Article

Cite This: ACS Appl. Mater. Interfaces 2019, 11, 11849−11856

www.acsami.org

# Enlarged Color Gamut Representation Enabled by Transferable Silicon Nanowire Arrays on Metal−Insulator−Metal Films

Yeong Jae Kim,[†] Young Jin Yoo,[†] Gil Ju Lee,[†] Dong Eun Yoo,[‡] Dong Wook Lee,[‡] Vantari Siva,[†] Hansung Song,[†] Il Suk Kang,*[,‡] and Young Min Song*[,†]

[†]School of Electrical Engineering and Computer Science, Gwangju Institute of Science and Technology, 123 Cheomdangwagi-ro, Buk-gu, Gwangju 61005, Republic of Korea

[‡]National Nanofab Center, Korea Advanced Institute of Science and Technology, 291 Daehak-ro, Yuseong-gu, Daejeon 34141, Republic of Korea.

Supporting Information

**ABSTRACT:** Artificial structural colors arising from nanosized materials have drawn much attention because of ultrahigh resolution, durability, and versatile utilizations compared to conventional pigments and dyes. However, the limited color range with current approaches has interrupted the supply for upcoming structural colorimetric applications. Here, we suggest a strategy for the widening of the color gamut by linear combination of two different resonance modes originating from silicon nanowire arrays (Si NWAs) and metal−insulator−metal nanoresonators. The enlarged color gamut representations are simply demonstrated by transferring Si NWAs embedded in a flexible polymer layer without additional treatment/fabrication. Optical simulation is used to verify the additive creation of a new resonance dip, without disturbing the original mode, and provides "predictable" color reproduction. Furthermore, we prove that the proposed structures are applicable to well-known semiconductor materials for various flexible optical devices and other colorant applications.

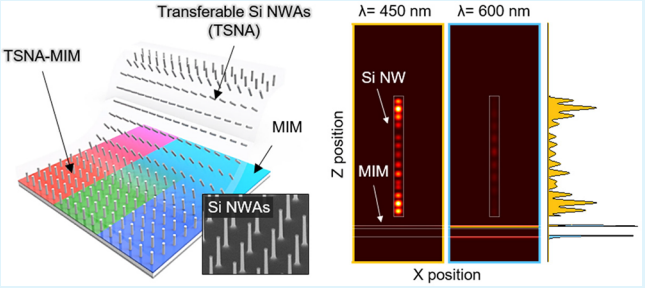


**KEYWORDS:** *silicon nanowire, transferable color filter, nanophotonics, structural coloration*

## INTRODUCTION

Structural coloration originates from the phenomena of light interaction in specific wavelength ranges of the visible spectrum, which can be modulated by controlling the geometrical parameters such as the diameter, period, shape, and environmental conditions.[1−6] To date, the specific light absorption features of organic pigments and dyes are commonly used to obtain color selectivity with mixing different color ingredients. However, these materials suffer from limitative resolution, environmental vulnerability such as chemicals and ultraviolet rays, and device compatibility.[7,8] Compared to traditional coloration approaches, nanostructural coloration mechanisms based on plasmonic nanostructures, metal−dielectric multilayers, and photonic crystals have been promoted for ultrahigh resolution and nonfading colors.[9−14] Furthermore, these types of color generation have attracted a great deal of attention in hopes of achieving future printing technologies for multipurpose utilization such as bright-field color prints, micro/nanosized steganography, anti-counterfeiting labels, nanoscale optical filters, refractive index sensing, and spectrally encoded optical data storage using their various structural functionalities.[10,15−34]

Among the various materials used for coloration, silicon (Si) is considered a strong candidate because of its remarkable advantages such as low cost, high stability, and well-developed fabrication methods.[35−37] In particular, Si nanostructures have been considered in structural coloration because of their selective absorptive properties, originating from light resonance effects such as leaky, guided, and Bloch modes.[2,38−47] Using the aforementioned properties, multicolor generation by silicon nanowire arrays (Si NWAs) has been successfully demonstrated for reflective/transmissive structural color filters.[16,43−45]

For more practical colorimetric applications, a linear combination of two or more resonance characteristics in each layer is required to extend expressible color ranges. The separation of hybrid resonances in patterned MIM structures has been previously reported to enhance the color gamut depending on the dielectric thickness and various metals in transmissive/reflective color filters.[25,26] Mixed nanodisks were demonstrated for color mixing properties.[48] However, the most complex multilayered structures are having difficulties in perfect linear combinations of additional reflectance dips at desired visible wavelengths.[10,49−54] Furthermore, colored

Received: December 9, 2018
Accepted: March 4, 2019
Published: March 4, 2019






DOI: 10.1021/acsami.8b21554
ACS Appl. Mater. Interfaces 2019, 11, 11849−11856

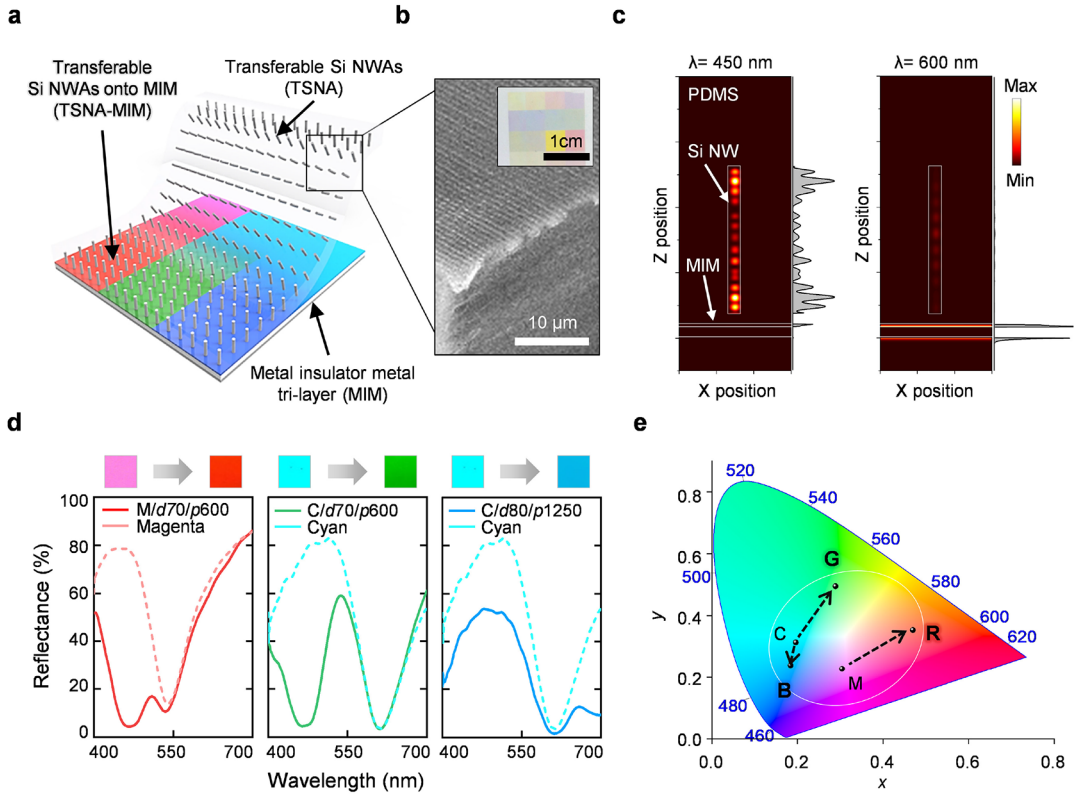


**Figure 1.** (a) Schematic illustration of TSNA-MIM (dashed area), TSNA, and MIM structures. (b) Tilted view of scanning electron microscopy (SEM) images for bottom side of TSNA and photographs of TSNA on white paper (inset). (c) Absorption profiles of green-colored TSNA-MIM filter at 450 and 600 nm wavelengths. (d) Bright-field microscopy images (MIM: top/left, TSNA-MIM: top/right) and measured reflectance spectra of MIM and TSNA-MIM with different diameters and periods of Si NWAs (i.e., $d$ = 70 nm, $p$ = 600 nm and $d$ = 80 nm, $p$ = 1250 nm) and insulator ($SiO_2$) thicknesses (i.e., 90, 120, and 150 nm) (lower). (e) Corresponding chromaticity coordinates from measured reflectance spectra in (d).

nanostructures have been precisely engineered by high-tech processes such as direct laser writing, electron beam lithography, and oblique angle deposition.[10−15] Despite full color generation achieved during last years, these approaches cannot be modifiable after color production.

To overcome the abovementioned issues, in this work, we present transferable silicon nanowire arrays embedded in a transparent polymer (TSNA) for enabling additive creation of reflectance dips to generate a widened color gamut without any resonance interaction between neighboring structures; this structure is easily transferable to other reflective colored filters. The hydrophobicity of the polydimethylsiloxane (PDMS) polymer leads to the passivation effect from external chemical reaction.[55] As a typical reflective color filter, the metal−insulator−metal (MIM) trilayer configuration, which provides subtractive colors generated by the Fabry−Pérot resonance, is employed to demonstrate the color mixing properties.[56−58] In the process, we designed and fabricated TSNA, MIM, and their TSNA-MIM combination for more versatile color reproduction. Furthermore, the enhanced color gamut representations of TSNA-MIM are discussed with the results of reflectance spectra analysis. Also, optical simulation results including reflectance contour maps, light absorption, and chromaticity diagrams with color representation support our concept more specifically. To verify the versatility of our method, we additionally performed theoretical analysis of the proposed structures with various high-index semiconductor materials.

## RESULTS AND DISCUSSION

Figure 1a exhibits a schematic representation of the transferable silicon nanowire arrays embedded in a transparent PDMS polymer (TSNA) on a metal−insulator−metal (MIM) nanoresonator (TSNA-MIM). This illustration shows the strategy for color shifts of the structure via stacking TSNA. The representative tilted surface morphology is obtained from field emission scanning electron microscopy (FE-SEM, Hitachi S-4700) of the TSNA, and the inset provides a photograph of the same (see Figure 1b). The diameters lie within the range of 60−110 nm necessary for generating resonant dips in the visible spectral range from 400 to 700 nm. The TSNA themselves act as a transparent band-stop filter at specific wavelength ranges with colors (inset of Figure 1b).[23−25] One interesting feature of this polymeric photonic film is that it is "transferable" to various foreign substrates because of PDMS stacking properties with flexibility. In this study, we particularly focus on color reproduction by stacking TSNA for various colored reflective filters. In conventional MIM structures consisting of the Ag/$SiO_2$/Ag multilayer, the three primary subtractive colors (i.e., cyan, magenta, and yellow) were generated by the Fabry−Pérot resonance, which have narrow bandwidth of an absorption spectrum. Thus, absorption band is shifted toward larger wavelengths with increasing cavity thickness (see Figure S1).[56−58] Figure 1c presents the absorption profile for a green-colored TSNA-MIM structure to confirm resonance independency of our proposed structure at 450 and 600 nm wavelengths. The TSNA with desired


DOI: 10.1021/acsami.8b21554
ACS Appl. Mater. Interfaces 2019, 11, 11849−11856

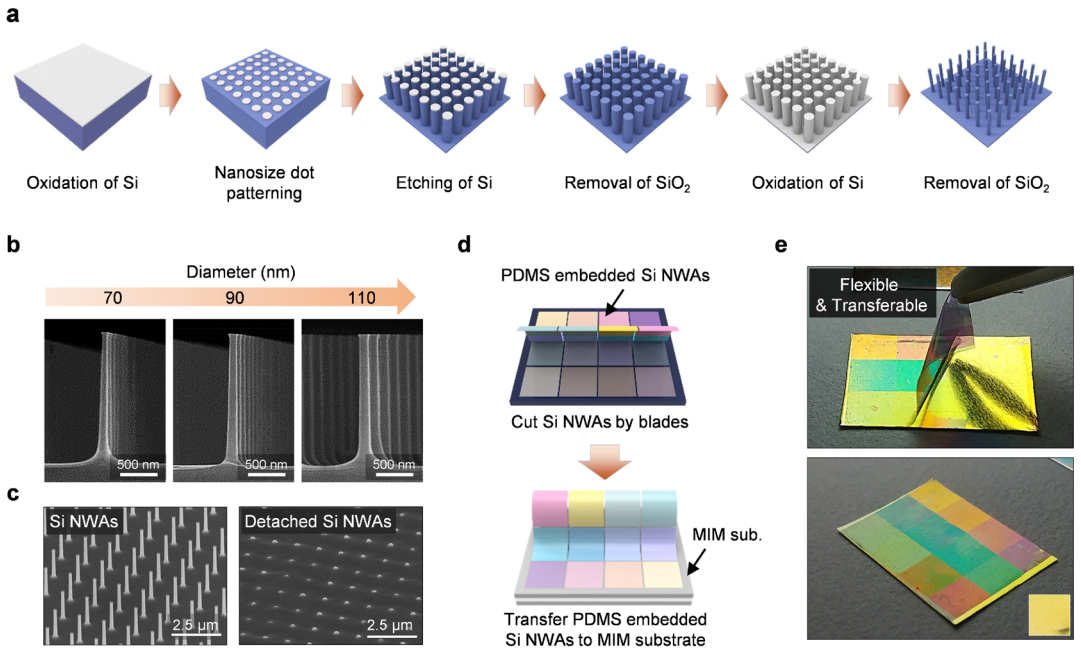


**Figure 2.** Schematic illustration for TSNA-MIM preparation steps. (a) Fabrication method for silicon nanowire arrays. (b) Cross-sectional SEM images of Si NWAs with the diameters of 70, 90, and 110 nm. (c) 45° tilted view SEM images of Si NWAs and detached Si NWAs. (d) Mechanical peeling off of PDMS embedded Si NWAs using blades (top) and transferring of Si NWAs embedded in flexible polymer onto colored films (bottom). (e) Photographs showing transferring process (top) and TSNA-MIM (bottom) with yellow background colors (bottom, inset).

geometry can provide a reflectance dip because of the HE11 mode at different wavelengths (e.g., 450 nm in this calculation).[43] On the other hand, MIM structures with an insulator ($SiO_2$) thickness of 150 nm afford a strong absorption at ~600 nm as shown in Figure 1c. The light in each structure strongly absorbs to form two reflectance dips at 450 and 600 nm without any loss. From these results, it proves that our proposed TSNA will be applied to optical devices requiring resonance selectivity. Bright-field microscopy images of representative samples (i.e., conventional MIM (top left) and combined TSNA-MIM structures (top right)) and their measured reflectance spectra are shown in Figure 1d. It is obvious that the additional reflectance dip drastically changes the presented colors from CM (dashed lines) to RGB (solid lines). In particular, it is observed that these two structures do not disrupt with each reflectance dip, which results in a linear combination of two different operational modes. This dramatic change in color alleviates the drawbacks of common MIM color filters and enhances the applicability in colorimetric purposes. Figure 1e shows CIE coordinates obtained from reflectance measurements. The color shifts and the enlarged color gamut occurred for combined structures corresponding to the results shown in Figure 1d.

Figure 2a shows the schemes of fabrication steps for Si NWAs. First, a Si substrate was thermally annealed to form a $SiO_2$ layer (~200 nm thick). Then, $SiO_2$ nanodisk arrays with different diameters (200−250 nm) were patterned in 10 nm increments by a KrF scanner lithography (Nikon Inc., KrF scanner S203-B). Si was etched (~2 $\mu$m deep) by a reactive ion etching anisotropically (RIE, Oxford Plasmalab 133). Hydrofluoric (HF) treatment was applied to remove $SiO_2$ residues, and the etched wafer was treated precisely with thermal oxidation (~60 nm thickness) to reduce the nanowire diameters from 60 to 110 nm. Finally, HF wet etching process was followed to remove the $SiO_2$ residues again. The fabricated vertical silicon nanowire arrays with different diameters were shown in Figure 2b. Polydimethylsiloxane (PDMS) polymer was prepared with a base to a curing agent ratio of 5:1 (Sylgard 184, Dow Corning Corporation, USA), which was under a vacuum for 30 min to remove air bubbles from a polymer. The PDMS layer was poured and spin coated with 1000 rpm for 60 s on the silicon nanowire substrate. To cure the PDMS layer, we annealed on a hot plate at 230 °C for 2 h. Then, natural curing was performed at room temperature for 3 h. After the PDMS polymer was cured, a blade (NT-Cutter, BSC-21P) was used as a sharp scraper to peel off the PDMS-embedded silicon nanowire arrays. Figure 2c shows the geometry information for silicon nanowire arrays (left) and detached nanowire arrays (right). Figure 2d illustrates the simple steps that were needed to transfer TSNA onto the MIM cavity. Finally, the TSNA was mounted on a MIM to arrive at our final TSNA-MIM structure. Figure 2e shows transferring process on MIM with color yellow, the TSNA has excellent flexibility and transferability (see Figure 2e, top). The photographs images for TSNA-MIM are shown in Figure 2e (bottom).

To understand the optical aspects of our proposed structure, the rigorous coupled-wave analysis (RCWA) was used to calculate varying diverse geometric parameters such as the nanowire diameter and cavity thickness using commercial software tools (DiffractMOD, RSoft Design Group, USA). In the calculations, the 15th diffraction order for RCWA and a grid size of 1 nm with periodic boundaries were used. The reflectance spectra and absorption profiles were simulated by averaging the TE and TM polarization modes. Material dispersions and extinction coefficients were considered for wavelength dependency. Commercial MATLAB (Mathworks, Inc.) software was used to calculate the chromatic information from the calculated and measured reflectance spectra.[59] The optical constants of semiconductor materials were taken from the previous literature.[60] First, we compare the MIMIM and


DOI: 10.1021/acsami.8b21554
ACS Appl. Mater. Interfaces 2019, 11, 11849−11856

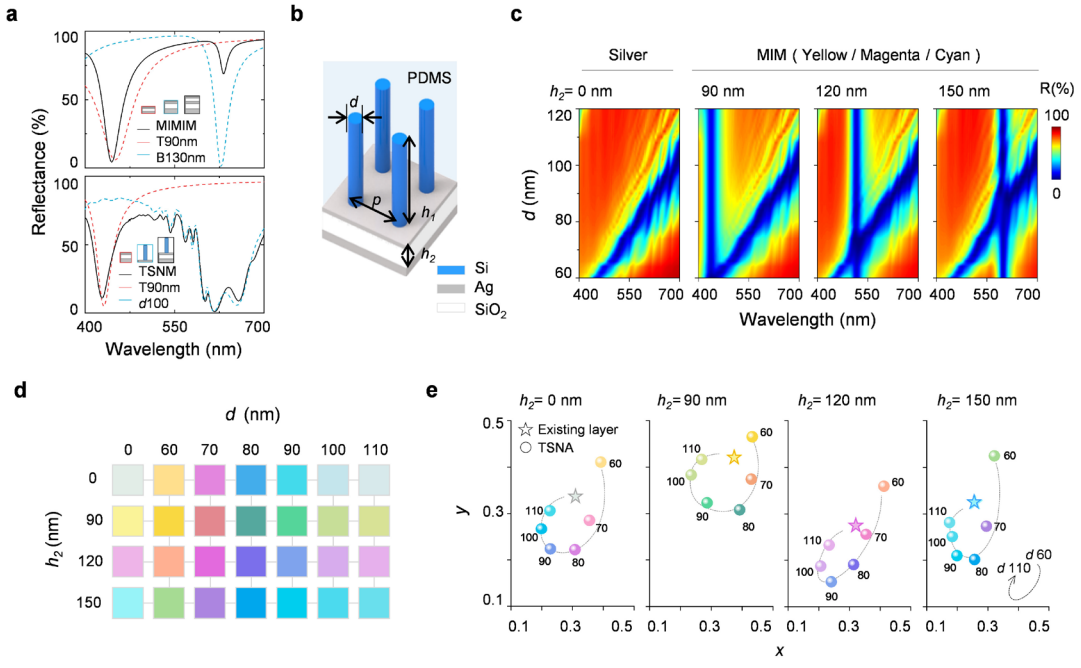


**Figure 3.** Simulation results for TSNA-MIM filter. (a) Comparison of MIMIM and TSNA-MIM filter. (b) Schematic illustration of PDMS embedded Si NWAs on MIM. (c) Contour plots of reflectance spectra with different cavity thicknesses: ($h_2$ = 0, 90, 120, and 150 nm) with fixed parameters for Si NWAs ($p$ = 1250 nm, $h_1$ = 2 $\mu$m). (d) Color representation from calculated results in (c). (e) Chromaticity diagrams corresponding to calculated results. The dashed arrow indicates increasing diameters of Si NWAs from 60 to 110 nm in 10 nm increments.

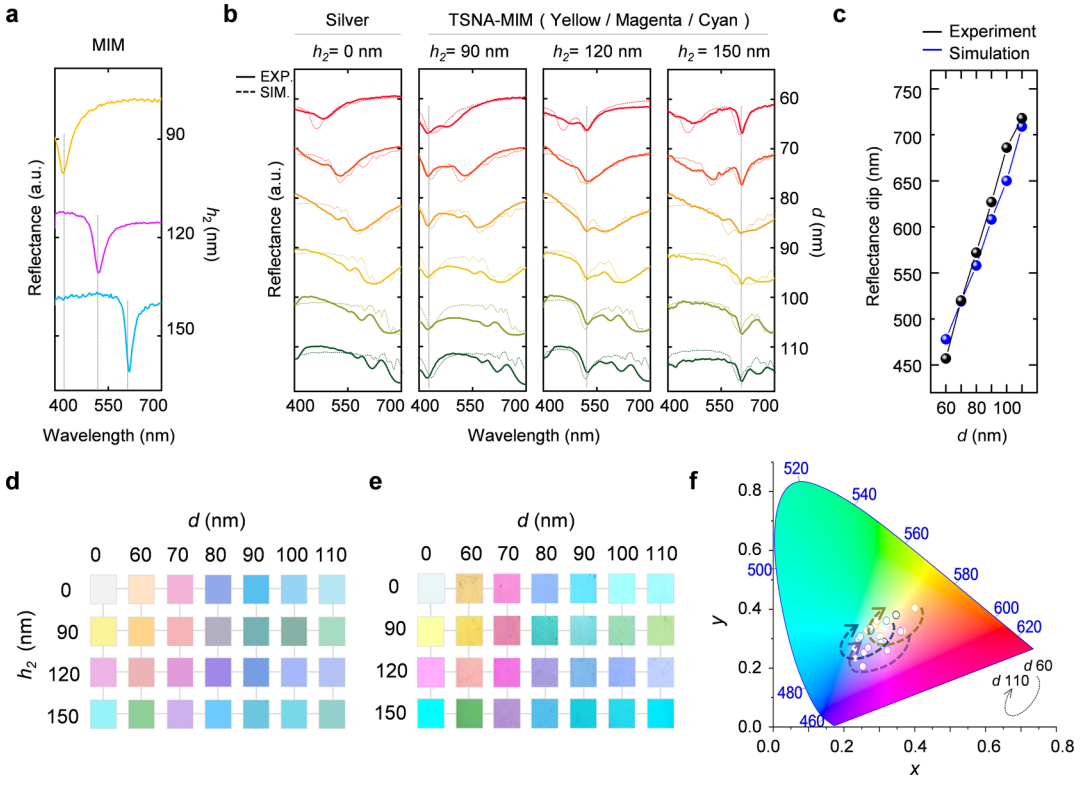


**Figure 4.** (a) Measured reflectance spectra for MIM with top layer Ag (30 nm)/$SiO_2$ (90, 120, and 150 nm)/Ag (100 nm) on Si substrate for yellow, magenta, and cyan colors, respectively. (b) Reflectance spectra for TSNA on silver and yellow-, magenta-, cyan-colored MIM (solid lines: measured reflectance and dotted lines: simulated reflectance). (c) Correlation between experimental and simulated reflectance dips with varying Si NWA diameters. (d) Color representation from measured reflectance spectra for TSNA-MIM. (e) Bright-field microscopy images for TSNA-MIM. (f) Chromaticity coordinates corresponding to reflectance spectra shown in (b). The dashed arrow indicates increasing diameters of Si NWAs from 60 to 110 nm in 10 nm increments.



DOI: 10.1021/acsami.8b21554
ACS Appl. Mater. Interfaces 2019, 11, 11849−11856

TSNA-MIM multilayers to uncover the difficulties in creating a new reflectance dips for an existing structure. In the case of MIMIM, the upper MIM (Ag (30 nm)/$SiO_2$ (90 nm)/Ag (30 nm)), the lower MIM (Ag (30 nm)/$SiO_2$ (130 nm)/Ag (100 nm)), and the MIMIM (Ag (30 nm)/$SiO_2$ (90 nm)/Ag (30 nm)/$SiO_2$ (130 nm)/Ag (100 nm)) were simulated. The strength of the reflectance dip in the top MIM was almost the same compared with that of the MIMIM at 410 nm wavelength, but the dip depth of the bottom MIM structure was decreased at 620 nm wavelength (Figure 3a, top). The light absorption occurs in the upper MIM layer, which hinders resonance in the lower MIM layer (see Figure S2). On the other hand, TSNA-MIM exhibits well-combined reflectance dips before/after combination. To further understand the applicable geometry of the TSNA-MIM parameters, additional optical simulations were carried out. Figure 3b provides a schematic illustration of the sample structure that was used for the simulations in which the parameters $d$, $p$, and $h_1$ represent the diameter, period, and height of the nanowire arrays, respectively. The parameter $h_2$ represents the insulator ($SiO_2$) thickness of the MIM. Contour maps of the simulated reflectance spectra as a function of wavelength and diameter of the nanowire, with constant values of period and height of nanowire ($p$ = 1250 nm and $h_1$ = 2 $\mu$m) for different thicknesses of cavities (i.e., $h_2$ = 0, 90, 120, and 150 nm), are shown in Figure 3c. It can be observed that the dip in reflectance spectra shifts to longer wavelengths with linear dependence on the diameter of the nanowire (see Figure 3c), which is in good agreement with the results reported by other works in the literature.[47] The reflectance dips for silicon nanowire arrays were found to shift with changes of height, period, refractive index, and air gap between TSNA and MIM (see Figure S3). Moreover, the angle properties are plotted in Figure S4. The periodic Si NWAs have diffraction characteristics with angle dependent coloration to the incidence light. These optically variable coloration effects are useful for security/authentication functions.[10,17,31−34] By increasing the cavity thicknesses ($h_2$ = 90, 120, and 150 nm for yellow, magenta, and cyan, respectively), the peaks were found to shift toward longer wavelengths ($\lambda$ = 410, 510, and 600 nm, respectively). It was further observed that the MIM structure and the TSNA do not disturb each other, which can be confirmed by their independent reflectance dips after stacking. The representative colors corresponding to these reflectance spectra for the different values of $d$ and $h_2$ were estimated. To consider our proposed structures in terms of coloration, we conducted a color representation, as displayed in Figure 3d, from the calculated reflectance (see Figure S5). It is worth mentioning that the colors of these structures can be variously tuned by playing with the parameters of the nanowires and the thickness of the cavity (see Figure 3d). To demonstrate the tunability of colors more quantitatively, the coordinates on the International Commission on Illumination (CIE) plots for the above structures are shown in Figure 3e. We note that all dashed curves rotate clockwise with an increasing diameter of the Si NWAs. Our structure can be realized in the wide color gamut through adjustment of Si NWA geometric parameters and $SiO_2$ thickness without changing materials.

We experimentally fabricated and measured reflectance spectra for MIM alone and TSNA-MIM structures (see Figure 4a,b). To obtain the desired reflection spectra for Si NWAs, diameters of 60 to 110 nm in 10 nm steps were used in these experiments. The top silver layer thickness was 30 nm to form vivid colors with the proper dip depth of reflectance. The reflectance dip is strongly generated as the absorption in the upper silver layer increases from 10 to 30 nm. However, more than 40 nm external light is reflected, and the effect of cavity is reduced (see Figure S1); the insulator layer thickness was varied to 90 nm for yellow, 120 nm for magenta, and 150 nm for cyan. The color can be adjusted according to the cavity thickness. The thickness was kept constant at 100 nm to exclude the light transmission. The diameters of the Si NWAs were changed from 60 to 110 nm in 10 nm increments. The creation of reflectance dips and peaks was significant for a color representation.[7,51,52] To compare with simulation results, simulated (dotted lines) and measured (solid lines) reflectance spectra are plotted in Figure 4b. The addition of the reflectance dips in the hybrid structures can be observed. It was confirmed that the dips changed only according to the diameter of the Si NWAs while the reflectance dips of the existing MIM structure were maintained. Figure 4c shows correlation between dips observed in the measured and simulation data. These tendencies for the reflectance dip that shifts varying diameters were almost consistent with the aforementioned simulation results. The colors were estimated from these measured reflectance spectra as shown in Figure 4d. From the results, it is possible to determine that the colors can be fine-tuned by adding the reflectance dips experimentally and changing the various parameters of the Si NWAs. Corresponding optical microscopy images are shown in Figure 4e. We note that the estimated colors and bright-field microscopy images are in very good agreement with each other. To demonstrate the enlarged color gamut, the standard CIE contour plots of these hybrid structures are shown in Figure 4f. Upon changing the diameter of the Si NWAs in the clockwise direction, the initial colors (cyan, magenta, and yellow) were found to change to a wide range of colors. To ensure versatility of the polymer-embedded structure, additional simulations were performed on various materials to show the possibility of color tunability. We chose four different well-known semiconducting materials: GaN, GaAs, SiGe, and Ge. We simulated the reflectance spectra of these different nanowires as a function of wavelength and diameter of the NWAs (see Figure 5a) while keeping the other parameters constant ($p$ = 1250 nm and $h_1$ = 2 $\mu$m). Interestingly, the reflectance dips follow the diameter dependence as in the present experimental results. For all the different materials, the corresponding colors as a function of diameter are shown in Figure 5b. The NWAs on MIM structures are shown in Figure S6. It may be observed that Ge and SiGe show less effect for the gamut range, whereas the GaAs and GaN materials offer much better gamut expansion. Standard CIE plots for all these materials are shown in Figure 5c. In the CIE plots, it is evident that the range of color tunability is in the order of low to high for Ge, SiGe, GaAs, Si, and GaN materials. The optical constants including refractive indices ($n$) and extinction coefficients ($k$) on the left and right axes, respectively, are shown in Figure S7. We note here that the extinction coefficients for the Ge, SiGe, GaAs, Si, and GaN materials with a high refractive index ($n$) are in decreasing order. This decreasing order of $k$ values can be attributed to the increasing order of the color tunability, which plays a crucial role in color generation. Also, the GaN-based coloration study offers more possible color tunability, and so Si-based technology can be promising due to its low cost/mature fabrication properties.


DOI: 10.1021/acsami.8b21554
ACS Appl. Mater. Interfaces 2019, 11, 11849−11856

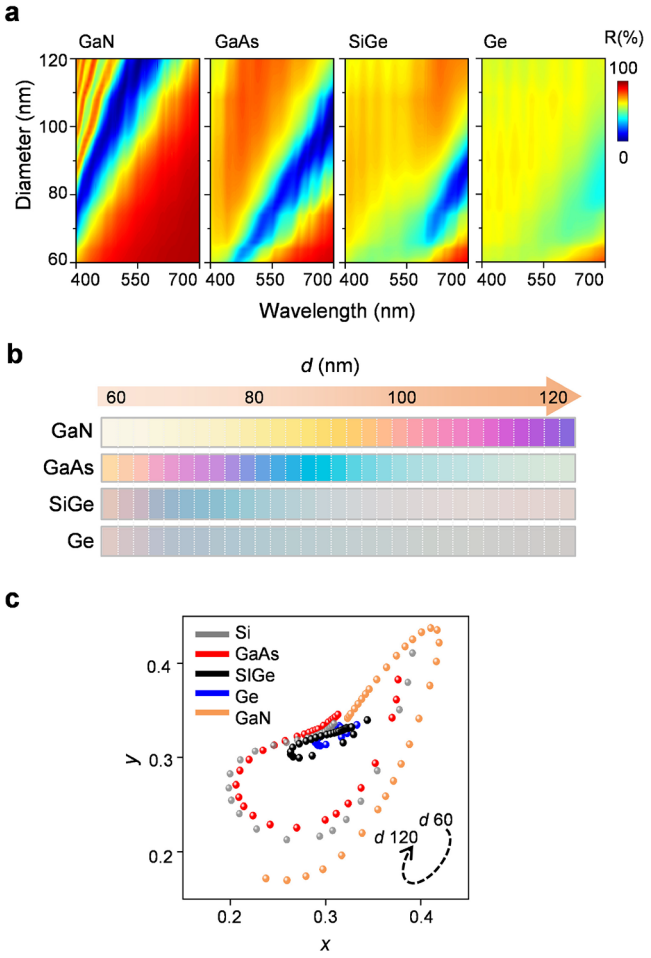


**Figure 5.** (a) Contour plots for reflectance spectra calculated from RCWA simulations for GaN, GaAs, SiGe, and Ge NWAs embedded in PDMS polymer on silver background. (b) Color representation. (c) Chromaticity coordinates corresponding to reflectance spectra shown in (a). The dashed arrow indicates increasing diameters of nanowire arrays from 60 to 120 nm in 10 nm increments.

## CONCLUSIONS

We have demonstrated the enhancement of color gamut expression by transferring the silicon nanowire arrays embedded in a flexible and transparent polymer. The silicon nanowire was adopted to selectively absorb the light in visible regions by modulating a geometric parameter such as diameters from 60 to 110 nm. We confirmed the color gamut tunability of the TSNA structure by stacking onto the cyan-, magenta-, and yellow-colored MIM reflective filter. Furthermore, we found that the independent phenomena of the two different resonances caused by silicon nanowire arrays and metal−insulator−metal films, which are difficult to realize in a general nanostructured multilayer. These results show that TSNA has independent wavelength selectivity, which is not affected by other light resonances. We also prove that polymer-embedded nanowire arrays are applicable to well-known semiconductor materials (i.e., GaN, GaAs, Ge, and SiGe) for various colorant applications. Using this approach, we believe that the enhanced color tunability and independent light resonance features of our proposed structures can be used as future color applications such as optical filters, security/anti-counterfeiting labels, and flexible decorative devices.

## ASSOCIATED CONTENT

### Supporting Information

The Supporting Information is available free of charge on the ACS Publications website at DOI: 10.1021/acsami.8b21554.

Additional optical simulation results for MIM, MIMIM, and silicon nanowire arrays; angle dependence properties of TSNA-MIM; reflectance properties and color representations for other semiconductor materials; CIE 1931 color space for color representation; and optical constants (PDF)

## AUTHOR INFORMATION

### Corresponding Authors

*E-mail: iskang@nnfc.re.kr (I.S.K.).
*E-mail: ymsong@gist.ac.kr (Y.M.S.).

### ORCID

Yeong Jae Kim: 0000-0002-0870-9044
Young Min Song: 0000-0002-4473-6883

### Notes

The authors declare no competing financial interest.

## ACKNOWLEDGMENTS

This work was supported by the Institute for Information & Communications Technology Promotion (IITP) (no.2017000709), the Creative Materials Discovery Program through the National Research Foundation of Korea (NRF) funded by the Korea government (MSIP) (NRF-2017M3D1A1039288, 2018H1A2A1060954,2018R1A4A1025623), GIST Research Institute(GRI) grant funded by the GIST in 2019, the Korea Institute of Energy Technology Evaluation and Planning(KETEP), and the Ministry of Trade, Industry & Energy(MOTIE) of the Republic of Korea (no. 20183010014310).

## REFERENCES

(1) Murray, W. A.; Barnes, W. L. Plasmonic Materials. *Adv. Mater.* **2007**, *19*, 3771−3782.
(2) Cao, L.; Fan, P.; Barnard, E. S.; Brown, A. M.; Brongersma, M. L. Tuning the Color of Silicon Nanostructures. *Nano Lett.* **2010**, *10*, 2649−2654.
(3) Sun, J.; Bhushan, B.; Tong, J. Structural Coloration in Nature. *RSC Adv.* **2013**, *3*, 14862−14889.
(4) Parker, A. R.; Townley, H. E. Biomimetics of Photonic Nanostructures. *Nat. Nanotechnol.* **2007**, *2*, 347.
(5) Gu, Y.; Zhang, L.; Yang, J. K. W.; Yeo, S. P.; Qiu, C.-W. Color Generation via Subwavelength Plasmonic Nanostructures. *Nanoscale* **2015**, *7*, 6409−6419.
(6) Steindorfer, M. A.; Schmidt, V.; Belegratis, M.; Stadlober, B.; Krenn, J. R. Detailed Simulation of Structural Color Generation Inspired by the Morpho Butterfly. *Opt. Express* **2012**, *20*, 21485−21494.
(7) Gilbert, P. U. P. A.; Haeberli, W. Experiments on Subtractive Color Mixing with a Spectrophotometer. *Am. J. Phys.* **2007**, *75*, 313−319.
(8) Kim, H.; Ge, J.; Kim, J.; Choi, S.-e.; Lee, H.; Lee, H.; Park, W.; Yin, Y.; Kwon, S. Structural Colour Printing Using a Magnetically Tunable and Lithographically Fixable Photonic Crystal. *Nat. Photonics* **2009**, *3*, 534.
(9) Cheng, F.; Gao, J.; Stan, L.; Rosenmann, D.; Czaplewski, D.; Yang, X. Aluminum Plasmonic Metamaterials for Structural Color Printing. *Opt. Express* **2015**, *23*, 14552−14560.
(10) Fan, J. R.; Wu, W. G.; Chen, Z. J.; Zhu, J.; Li, J. Three-Dimensional Cavity Nanoantennas with Resonant-Enhanced Surface


DOI: 10.1021/acsami.8b21554
ACS Appl. Mater. Interfaces 2019, 11, 11849−11856

Plasmons as Dynamic Color-Tuning Reflectors. *Nanoscale* **2017**, *9*, 3416−3423.
(11) Yoo, Y. J.; Lim, J. H.; Lee, G. J.; Jang, K.-I.; Song, Y. M. Ultra-Thin Films with Highly Absorbent Porous Media Fine-Tunable for Coloration and Enhanced Color Purity. *Nanoscale* **2017**, *9*, 2986−2991.
(12) Vorobyev, A. Y.; Guo, C. Colorizing Metals with Femtosecond Laser Pulses. *Appl. Phys. Lett.* **2008**, *92*, No. 041914.
(13) Guay, J.-M.; Lesina, A. C.; Côté, G.; Charron, M.; Poitras, D.; Ramunno, L.; Berini, P.; Weck, A. Laser-Induced Plasmonic Colours on Metals. *Nat. Commun.* **2017**, *8*, 16095.
(14) Nagasaki, Y.; Suzuki, M.; Hotta, I.; Takahara, J. Control of Si-Based All-Dielectric Printing Color through Oxidation. *ACS Photonics* **2018**, *5*, 1460−1466.
(15) Clausen, J. S.; Højlund-Nielsen, E.; Christiansen, A. B.; Yazdi, S.; Grajower, M.; Taha, H.; Levy, U.; Kristensen, A.; Mortensen, N. A. Plasmonic Metasurfaces for Coloration of Plastic Consumer Products. *Nano Lett.* **2014**, *14*, 4499−4504.
(16) Flauraud, V.; Reyes, M.; Paniagua-Domínguez, R.; Kuznetsov, A. I.; Brugger, J. Silicon Nanostructures for Bright Field Full Color Prints. *ACS Photonics* **2017**, *4*, 1913−1919.
(17) Jiang, H.; Kaminska, B. Scalable Inkjet-Based Structural Color Printing by Molding Transparent Gratings on Multilayer Nanostructured Surfaces. *ACS Nano* **2018**, *12*, 3112−3125.
(18) Heydari, E.; Sperling, J. R.; Neale, S. L.; Clark, A. W. Plasmonic Color Filters as Dual-State Nanopixels for High-Density Microimage Encoding. *Adv. Funct. Mater.* **2017**, *27*, 1701866.
(19) Yang, D.; Ye, S.; Ge, J. Old Relief Printing Applied to the Current Preparation of Multi-Color and High Resolution Colloidal Photonic Crystal Patterns. *Chem. Commun.* **2015**, *51*, 16972−16975.
(20) Murthy, S.; Pranov, H.; Feidenhans'l, N. A.; Madsen, J. S.; Hansen, P. E.; Pedersen, H. C.; Taboryski, R. Plasmonic Color Metasurfaces Fabricated by a High Speed Roll-To-Roll Method. *Nanoscale* **2017**, *9*, 14280−14287.
(21) Hu, D.; Lu, Y.; Cao, Y.; Zhang, Y.; Xu, Y.; Li, W.; Gao, F.; Cai, B.; Guan, B.-O.; Qiu, C.-W.; Li, X. Laser-Splashed Three-Dimensional Plasmonic Nanovolcanoes for Steganography in Angular Anisotropy. *ACS Nano* **2018**, *12*, 9233−9239.
(22) Xue, J.; Zhou, Z.-K.; Wei, Z.; Su, R.; Lai, J.; Li, J.; Li, C.; Zhang, T.; Wang, X.-H. Scalable, Full-Colour and Controllable Chromotropic Plasmonic Printing. *Nat. Commun.* **2015**, *6*, 8906.
(23) Duan, X.; Kamin, S.; Liu, N. Dynamic Plasmonic Colour Display. *Nat. Commun.* **2017**, *8*, 14606.
(24) Chen, Q.; Cumming, D. R. S. High Transmission and Low Color Cross-Talk Plasmonic Color Filters Using Triangular-lattice Hole Arrays in Aluminum Films. *Opt. Express* **2010**, *18*, 14056−14062.
(25) Lu, B. R.; Xu, C.; Liao, J.; Liu, J.; Chen, Y. High-Resolution Plasmonic Structural Colors from Nanohole Arrays with Bottom Metal Disks. *Opt. Lett.* **2016**, *41*, 1400−1403.
(26) Roberts, A. S.; Pors, A.; Albrektsen, O.; Bozhevolnyi, S. I. Subwavelength Plasmonic Color Printing Protected for Ambient Use. *Nano Lett.* **2014**, *14*, 783−787.
(27) Ditlbacher, H.; Krenn, J. R.; Lamprecht, B.; Leitner, A.; Aussenegg, F. R. Spectrally Coded Optical Data Storage by Metal Nanoparticles. *Opt. Lett.* **2000**, *25*, 563−565.
(28) Goh, X. M.; Zheng, Y.; Tan, S. J.; Zhang, L.; Kumar, K.; Qiu, C.-W.; Yang, J. K. W. Three-Dimensional Plasmonic Stereoscopic Prints in Full Colour. *Nat. Commun.* **2014**, *5*, 5361.
(29) Kumar, K.; Duan, H.; Hegde, R. S.; Koh, S. C. W.; Wei, J. N.; Yang, J. K. W. Printing Colour at the Optical Diffraction Limit. *Nat. Nanotechnol.* **2012**, *7*, 557.
(30) Wu, Y.-K. R.; Hollowell, A. E.; Zhang, C.; Guo, L. J. Angle-Insensitive Structural Colours Based on Metallic Nanocavities and Coloured Pixels beyond the Diffraction Limit. *Sci. Rep.* **2013**, *3*, 1194.
(31) Peng, C.-Y.; Hsu, C.-W.; Li, C.-W.; Wang, P.-L.; Jeng, C.-C.; Chang, C.-C.; Wang, G.-J. Flexible Photonic Crystal Material for Multiple Anticounterfeiting Applications. *ACS Appl. Mater. Interfaces* **2018**, *10*, 9858−9864.
(32) Meng, Y.; Qiu, J.; Wu, S.; Ju, B.; Zhang, S.; Tang, B. Biomimetic Structural Color Films with a Bilayer Inverse Heterostructure for Anticounterfeiting Applications. *ACS Appl. Mater. Interfaces* **2018**, *10*, 38459−38465.
(33) Wu, S.; Liu, B.; Su, X.; Zhang, S. Structural color patterns on paper fabricated by inkjet printer and their application in anticounterfeiting. *J. Phys. Chem. Lett.* **2017**, *8*, 2835−2841.
(34) Walia, J.; Dhindsa, N.; Khorasaninejad, M.; Saini, S. S. Color generation and refractive index sensing using diffraction from 2D silicon nanowire arrays. *Small* **2014**, *10*, 144−151.
(35) Rey, B. M.; Elnathan, R.; Ditcovski, R.; Geisel, K.; Zanini, M.; Fernandez-Rodriguez, M.-A.; Naik, V. V.; Frutiger, A.; Richtering, W.; Ellenbogen, T.; Voelcker, N. H.; Isa, L. Fully Tunable Silicon Nanowire Arrays Fabricated by Soft Nanoparticle Templating. *Nano Lett.* **2016**, *16*, 157.
(36) Chen, Z. X.; Yu, H. Y.; Singh, N.; Shen, N. S.; Sayanthan, R. D.; Lo, G. Q.; Kwong, D.-L. Demonstration of Tunneling FETs Based on Highly Scalable Vertical Silicon Nanowires. *IEEE Electron Device Lett.* **2009**, *30*, 754−756.
(37) Teng, F.; Li, N.; Xu, D.; Xiao, D.; Yang, X.; Lu, N. Precise Regulation of Tilt Angle of Si Nanostructures via Metal-Assisted Chemical Etching. *Nanoscale* **2017**, *9*, 449−453.
(38) Chern, W.; Hsu, K.; Chun, I. S.; de Azeredo, B. P.; Ahmed, N.; Kim, K.-H.; Zuo, J.-m.; Fang, N.; Ferreira, P.; Li, X. Nonlithographic Patterning and Metal-Assisted Chemical Etching for Manufacturing of Tunable Light-Emitting Silicon Nanowire Arrays. *Nano Lett.* **2010**, *10*, 1582−1588.
(39) Garnett, E.; Yang, P. Light Trapping in Silicon Nanowire Solar Cells. *Nano Lett.* **2010**, *10*, 1082−1087.
(40) Fountaine, K. T.; Whitney, W. S.; Atwater, H. A. Resonant Absorption in Semiconductor Nanowires and Nanowire Arrays: Relating Leaky Waveguide Modes to Bloch Photonic Crystal Modes. *J. Appl. Phys.* **2014**, *116*, 153106.
(41) Abujetas, D. R.; Paniagua-Domínguez, R.; Sánchez-Gil, J. A. Unraveling the Janus Role of Mie Resonances and Leaky/Guided Modes in Semiconductor Nanowire Absorption for Enhanced Light Harvesting. *ACS Photonics* **2015**, *2*, 921−929.
(42) Kuznetsov, A. I.; Miroshnichenko, A. E.; Brongersma, M. L.; Kivshar, Y. S.; Luk'yanchuk, B. Optically Resonant Dielectric Nanostructures. *Science* **2016**, *354*, aag2472.
(43) Seo, K.; Wober, M.; Steinvurzel, P.; Schonbrun, E.; Dan, Y.; Ellenbogen, T.; Crozier, K. B. Multicolored Vertical Silicon Nanowires. *Nano Lett.* **2011**, *11*, 1851−1856.
(44) Park, H.; Dan, Y.; Seo, K.; Yu, Y. J.; Duane, P. K.; Wober, M.; Crozier, K. B. Filter-Free Image Sensor Pixels Comprising Silicon Nanowires with Selective Color Absorption. *Nano Lett.* **2014**, *14*, 1804−1809.
(45) Park, H.; Crozier, K. B. Multispectral Imaging with Vertical Silicon Nanowires. *Sci. Rep.* **2013**, *3*, 2460.
(46) Park, H.; Seo, K.; Crozier, K. B. Adding Colors to Polydimethylsiloxane by Embedding Vertical Silicon Nanowires. *Appl. Phys. Lett.* **2012**, *101*, 193107.
(47) Khorasaninejad, M.; Abedzadeh, N.; Walia, J.; Patchett, S.; Saini, S. S. Color Matrix Refractive Index Sensors Using Coupled Vertical Silicon Nanowire Arrays. *Nano Lett.* **2012**, *12*, 4228−4234.
(48) Miyata, M.; Hatada, H.; Takahara, J. Full-Color Subwavelength Printing with Gap-Plasmonic Optical Antennas. *Nano Lett.* **2016**, *16*, 3166−3172.
(49) Li, Y.; Luo, D.; Peng, Z. H. Full-Color Reflective Display Based on Narrow Bandwidth Templated Cholesteric Liquid Crystal Film. *Opt. Mater. Express* **2017**, *7*, 16−24.
(50) Jalali, M.; Yu, Y.; Xu, K.; Ng, R. J. H.; Dong, Z.; Wang, L.; Dinachali, S. S.; Hong, M.; Yang, J. K. W. Stacking of Colors in Exfoliable Plasmonic Superlattices. *Nanoscale* **2016**, *8*, 18228−18234.
(51) Xiang, J.; Li, Y.; Li, Q.; Paterson, D. A.; Storey, J. M. D.; Imrie, C. T.; Lavrentovich, O. D. Electrically Tunable Selective Reflection of Light from Ultraviolet to Visible and Infrared by Heliconical Cholesterics. *Adv. Mater.* **2015**, *27*, 3014−3018.


DOI: 10.1021/acsami.8b21554
*ACS Appl. Mater. Interfaces* 2019, 11, 11849−11856

(52) Wang, H.; Wang, X.; Yan, C.; Zhao, H.; Zhang, J.; Santschi, C.; Martin, O. J. F. Full Color Generation Using Silver Tandem Nanodisks. *ACS Nano* **2017**, *11*, 4419−4427.
(53) Fleischman, D.; Sweatlock, L. A.; Murakami, H.; Atwater, H. Hyper-Selective Plasmonic Color Filters. *Opt. Express* **2017**, *25*, 27386−27395.
(54) James, T. D.; Mulvaney, P.; Roberts, A. The Plasmonic Pixel: Large Area, Wide Gamut Color Reproduction Using Aluminum Nanostructures. *Nano Lett.* **2016**, *16*, 3817−3823.
(55) Zhang, X.-S.; Zhu, F.-Y.; Han, M.-D.; Sun, X.-M.; Peng, X.-H.; Zhang, H.-X. Self-Cleaning Poly (dimethylsiloxane) Film with Functional Micro/Nano Hierarchical Structures. *Langmuir* **2013**, *29*, 10769−10775.
(56) Diest, K.; Dionne, J. A.; Spain, M.; Atwater, H. A. Tunable Color Filters Based on Metal−Insulator− Metal Resonators. *Nano Lett.* **2009**, *9*, 2579−2583.
(57) Li, Z.; Butun, S.; Aydin, K. Large-Area, Lithography-Free Super Absorbers and Color Filters at Visible Frequencies Using Ultrathin Metallic Films. *ACS Photonics* **2015**, *2*, 183−188.
(58) Lee, G. J.; Kim, Y. J.; Kim, H. M.; Yoo, Y. J.; Song, Y. M. Colored, Daytime Radiative Coolers with Thin-Film Resonators for Aesthetic Purposes. *Adv. Opt. Mater.* **2018**, *6*, 1800707.
(59) Ohta, N.; Robertson, A. CIE Standard Colorimetric System. In *Colorimetry: Fundamentals and Applications*; John Wiley & Sons, Ltd.: Chichester, UK, 2005.
(60) Palik, E. D. *Handbook of Optical Constants of Solids*; 1st ed.; Academic Press: New York, 1985.


DOI: 10.1021/acsami.8b21554
*ACS Appl. Mater. Interfaces* 2019, 11, 11849−11856